

Review

d^0 Ferromagnetism of Magnesium Oxide

Jitendra Pal Singh *  and Keun Hwa Chae * 

Advanced Analysis Centre, Korea Institute of Science and Technology, Seoul 02792, Korea

* Correspondence: jitendra_singh2029@kist.re.kr (J.P.S.); khchae@kist.re.kr (K.H.C.);

Tel.: +82-5427-91503 (J.P.S.); +82-5427-91192 (K.H.C.)

Received: 2 August 2017; Accepted: 22 November 2017; Published: 29 November 2017

Abstract: Magnetism without d-orbital electrons seems to be unrealistic; however, recent observations of magnetism in non-magnetic oxides, such as ZnO, HfO₂, and MgO, have opened new avenues in the field of magnetism. Magnetism exhibited by these oxides is known as d^0 ferromagnetism, as these oxides either have completely filled or unfilled d-/f-orbitals. This magnetism is believed to occur due to polarization induced by p-orbitals. Magnetic polarization in these oxides arises due to vacancies, the excitation of trapped spin in the triplet state. The presence of vacancies at the surface and subsurface also affects the magnetic behavior of these oxides. In the present review, origins of magnetism in magnesium oxide are discussed to obtain understanding of d^0 ferromagnetism.

Keywords: d^0 ferromagnetism; MgO; polarization; defects

1. Introduction

Magnetism is a well-established phenomenon which arises due to the exchange interaction between the electrons in partially-filled d-/f-bands in materials. Thus, materials with partially-filled d-/f-orbitals exhibit this phenomenon [1–3]. Apart from this, magnetic behavior of certain materials with completely-filled or zero-filled d-/f-shells is also observed and has remained under debate among researchers during the last decade [4–10].

Magnetism which arises due to completely-filled or unfilled d-/f-orbitals is known as d^0 ferromagnetism and is a wide field of study for the scientific community from a phenomenological point of view [4–8]. To date, this magnetism is observed in a variety of materials with different sources of origin and is classified accordingly [11–25].

Room-temperature ferromagnetism (RTFM) in pure sodium chloride particles is attributed to surface defects [11]. Carbon dangling bonds/vacancies are responsible for RTFM in polymers and carbon-based molecular materials [12–14]. RTFM in Ca- and Mg-stabilized zirconia is ascribed to oxygen vacancies [15]. Moreover, oxygen vacancies associated with misfit stress at the film substrate interface in SnO₂, CeO₂, Al₂O₃, ZnO, MgO, and HfO₂ thin films are responsible for RTFM [16]. Vacancy mediated magnetism occurs in CuO [17] and ZnO [18,19]; oxygen vacancy induced magnetism in zinc peroxide [20] and CeO₂ [21]; and surface vacancy induced magnetism in NiO [22]. Thus, these studies reveal that defects in the form of vacancies are the source of this behavior [11–22], however, sustainability of this magnetism up to long-range order requires exigency of the mechanism of interaction among these sources. It was observed that this kind of magnetism is governed by the double exchange mechanism through p-p interactions in Mg-doped SnO₂ [23], as well as B-, C-, and N-doped BeO systems [24]. Charge transfer between Mn²⁺ and Mn³⁺ states of Mn ions and the local density of states associated with extended structural defects form a net magnetic moment in Mn-doped In₂O₃ [25]. In case of HfO₂, high-spin defect states in isolated cation vacancy sites couple ferromagnetically with short-range magnetic interaction to establish a ferromagnetic ground state [26]. Thus d^0 ferromagnetism can not only be interpreted in terms of vacancies/defects, but understanding of appropriate mechanism revealing the interaction that leads to existence of such an effect upto

long-range order is another aspect [11–25]. Hence, investigation of the nature of magnetic interaction, along with the nature of defects in these materials, are important to understand the concept of d^0 ferromagnetism. In lieu of providing concise and concrete understanding of the field, it will be crucial to discuss these aspects for a well-known simple system.

Here, we attempt to give simple introduction to the issues related to d^0 ferromagnetism by taking magnesium oxide as an example. In the following section, conventional and emerging properties of MgO are discussed by giving a brief description of their importance in the field of d^0 ferromagnetism. Thereafter, sections are dedicated to experimental observations of magnetism in MgO. In the following section sources of magnetism in this material are discussed in terms of theoretical background. At the end, we have elaborated the results obtained from recent studies of our group.

2. Magnesium Oxide

2.1. Electronic Configuration and Structure

Magnesium oxide is a well-known inorganic material. It has molar mass of $40.31 \text{ gm}\cdot\text{mol}^{-1}$ and a density of $3.58 \text{ gm}\cdot\text{cm}^{-3}$ [27]. The constituents of this material are Mg^{2+} and O^{2-} ions. The electronic configurations of these ions are $1s^22s^2p^6$ and $1s^22s^2p^6$, respectively (Figure 1a) [28]. Thus, d-orbitals in this material are empty.

This material exhibits a rock-salt structure. The unit cell of this material is described as two interpenetrating face centered cubic (FCC) lattices, one of Mg and one of O, displaced from each other by 0.5 of the body diagonal (Figure 1b). Mg cations in the structure are surrounded by an octahedron of six O anions in perfect MgO. The symmetry of this octahedron crystal field belongs to O_h . The crystalline phase of this material is stable upto 227 GPa. Above this pressure its structure transforms to CsCl structure [29]. The lattice parameter for the rock-salt phase MgO is 4.212 \AA [30].

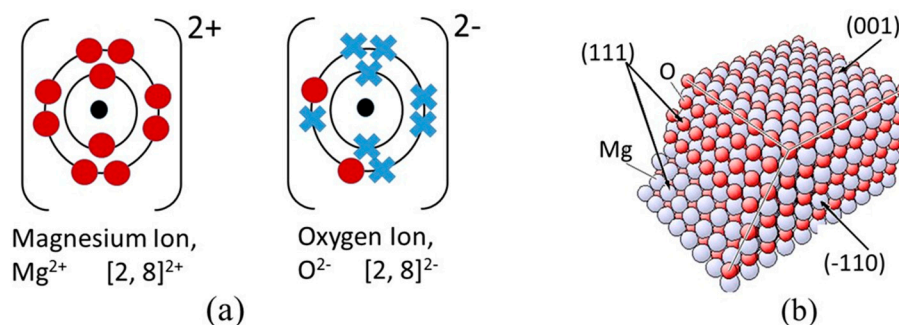


Figure 1. (a) Electronic configuration of Mg^{2+} and O^{2-} ions, and (b) crystal structure of MgO. Values in parenthesis represents (hkl) planes.

2.2. General Properties

Absence of free electron makes this material a good insulator whose resistivity varies up to $10^{18} \text{ ohm}\cdot\text{cm}$ [31,32]. Charge carriers induced by light in the various absorption bands of this material show onset of the photo-induced Hall Effect [33]. The room-temperature fundamental absorption in this material occurs at 7.6 eV with a probable second peak at 8.8 eV [34]. The dielectric constant of this material is 10 [35]. Thus, highly-insulating nature of this material, provides an opportunity to be utilized in fabrication of magnetic tunnel junctions, an important spintronic device [36].

2.3. Emerging Phenomena at Low Dimensions

The dielectric constant of this material increases to almost three orders of magnitude for peashell-like MgO nanostructures [37]. MgO nanoparticles exhibit almost 10% reflectance in the UV–VIS range which is almost 100% for bulk MgO. This value of reflectance corresponds to the optical

band gap of 2.8 eV for MgO nanoparticles (Figure 2) [38]. Room-temperature broadband laser emission in the near-ultraviolet to the blue-green spectral range is also observed in this material [39].

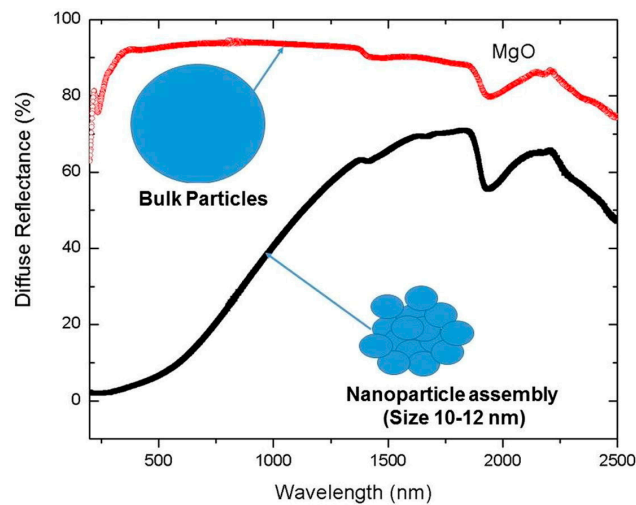


Figure 2. Diffuse reflectance spectra of MgO nanoparticle and bulk [38].

Apart from modified dielectric and optical behavior, RTFM in this material is also observed. Figure 3 shows the hysteresis curves of MgO thin films of thickness 8 (MgO-1) and 52 nm (MgO-2) at 300 K and 10 K [40]. These hysteresis curves reflect d^0 ferromagnetic behavior. More interestingly, spin-dependent electron reflection for MgO thin films grown on Fe(001) exhibit quantum interference [41]. Ferromagnetism combining with multilevel switching characteristics in MgO capacitor is also observed which might pave the way for a new method for spintronic multibit data storage [42]. Thus, these interesting dielectric, optical and magnetic phenomena make this material more relevant in current scenario.

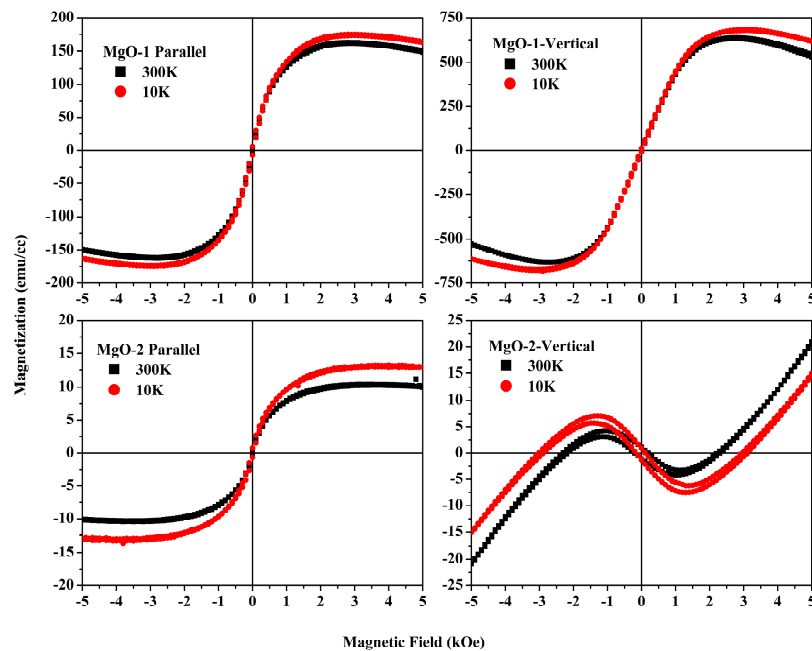


Figure 3. M-H curves of MgO-1 and MgO-2 thin films at 300 K and 10 K in the magnetic field applied in perpendicular (vertical) and parallel (parallel) directions to the film surface. Thickness of MgO-1 and MgO-2 is 8 and 52 nm respectively [40].

Since, this material has no electrons present in d-orbitals of any of its constituent ions, it may be considered as a prototype material for understanding d^0 ferromagnetism. To get better insights of various aspects, magnetism of MgO will be elaborated based on both experimental and theoretical approaches in the next two sections.

3. Magnetism of MgO: Experimental Approach

As discussed in previous sections, RTFM in these kind of materials is induced/affected by vacancies/defects. Hence, this section discusses the magnetism induced by extrinsic and intrinsic defects. Extrinsic defects are due to the presence of dopant ions in the lattice, and intrinsic defects are those created during deposition and annealing of films/nanoparticles. Thus, this section is dedicated to elaborate the results obtained for MgO doped with magnetic and non-magnetic ions along with pure MgO.

3.1. Doping with Magnetic Ions

To induce defects/vacancies inside MgO lattice different kinds of ions were utilized. No doubt doping with magnetic ions in MgO leads to a magnetic effect, however, defects still play an important role, as described for various material of this class [11–22].

Weak RTFM in MgO doped with 1% ^{57}Fe is ascribed to the interstitial defects when synthesized below a certain temperature (800 °C). Above this temperature, the formation of the core and shell of fine MgFe_2O_4 grains diluted in MgO matrix is responsible for this effect [43]. A similar effect was observed for MgO doped with Ni, which exhibits paramagnetism rather than RTFM in the absence of intrinsic defects, such as vacancies and interstitials [44]. Moreover, weak RTFM of MgO single crystals doped with Ni and Co are ascribed to the presence of O^{2-} vacancies produced during film growth [45]. MgO implanted with N and Fe atoms with a dose of 1×10^{18} ions/cm² exhibit RTFM. These authors have also shown that annealing reduces this behavior implying the role of vacancies in determining RTFM [46].

3.2. Doping with Non-Magnetic Ions

Apart from magnetism observed in MgO doped with magnetic elements, the effect was also observed in materials when doped with non-magnetic ions [47–50]. The appearance of RTFM in this material is reported when doped by nonmagnetic Zn [47] and Al [48]. This behavior is ascribed to cation (zinc) vacancies in the first case [47] and to oxygen vacancies in other cases [48]. RTFM in MgO single crystals, implanted with 70 keV O ions with respective doses of 2×10^{16} and 2×10^{17} ions/cm² is associated with presence of Mg vacancies, however, implantation of C or N instead of oxygen plays a more effective role in ferromagnetic performance than Mg vacancies [49]. In a recent study, in our group, the presence of magnetic ordering in MgO (100) single crystals implanted with N ions at two different fluence doses of 5×10^{16} and 1×10^{17} ions/cm² was also observed. We observed that saturation magnetization increases at higher fluence [50]. Thus, these studies show that RTFM is induced by the defects rather than the nature of dopant ions. To further corroborate the role of defects on RTFM, magnetic behavior of pure MgO is discussed in the next section.

3.3. Non-Doped Systems

Arajua et al. [51] have shown that saturation magnetization (M_s) of 170 nm thick MgO film grown using RF-sputtering is 5.7 emu/cm³. These authors also observed thickness dependent transition from ferromagnetic to paramagnetic state in pure MgO thin films [51]. Magnetization of 170 nm film is suppressed at higher oxygen pressure which reflects role of cation vacancies [52]. Cation vacancies induced RTFM are also observed in homogeneously (200) oriented MgO ~85 nm thin film deposited on Si substrates by inkjet printing [53] and MgO thin films deposited by pulsed laser deposition [54]. Mg vacancies induced RTFM have also been observed in MgO nanoparticles [55,56]. Large concentration of Mg vacancies at the surfaces of nano-grains establish magnetic percolation in

MgO nanoparticles [57], as well as thin films [58]. Thus, the magnetic behavior of MgO is induced by cation vacancies, however, Kumar et al. reported the role of oxygen vacancies to induce the RTFM spin-order in MgO nano-crystallites (Figure 4) [59].

A similar explanation is given for highly-defective MgO nanosheets prepared by colloidal synthesis. These nanosheets consist of strongly-interacting spin clusters which disappeared upon high-temperature annealing. These spins are concentrated along extended defects, possibly as unpaired electrons trapped at oxygen vacancies [60]. Saturation magnetization of MgO decrease with time at ambient atmosphere and it can be successively switched on again by annealing these films in vacuum [61]. Thus, experimental results explain that magnetism of pure MgO is induced by Mg vacancies, however, spin species trapped along-with oxygen vacancies also stabilize RTFM in MgO thin films.

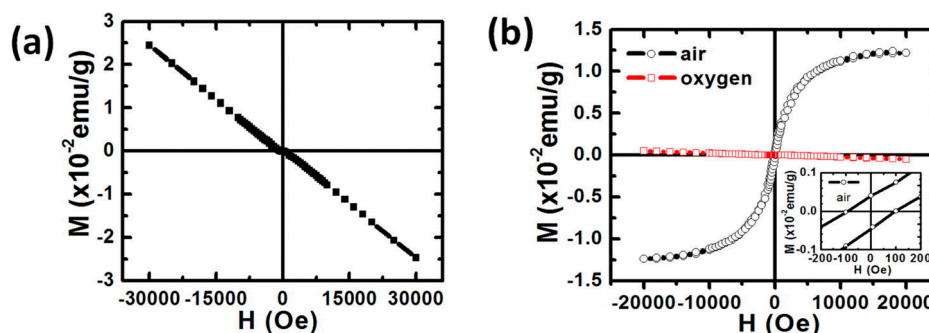


Figure 4. Room-temperature magnetization curves of MgO nanocrystallites synthesized at the calcination temperature of (a) 1000 °C in air and (b) 600 °C air and oxygen for 2 h each [59].

4. Magnetism of MgO: Theoretical Approach

4.1. Mg Vacancy as a Source of Magnetism

Theoretical simulations reveal that introduction of Mg vacancies into MgO favors the stabilization of half-metallic ferromagnetism [62–64]. This aspect is in correlation with experimental results obtained from various experimental studies [51–58]. Mg vacancies help to retain local magnetic moments in this material irrespective of the concentration [63–69]. The origin of magnetic moments associated with Mg vacancies is explained as follows:

It is observed that Mg vacancies do not affect to the O_h symmetry of MgO lattice. However, two dominant effects occur in this system assisted by this vacancy-(1) formation of charged defects and (2) slight modification of the Mg–O distance. These effects lead to the splitting of σ -type molecular orbitals into singlet a_{1g} , triplet, and doublet e_g states, as described in Figure 5. On the basis of occupancy of e_g states that net spin of perfect MgO, V_{Mg}^0 , V_{Mg}^+ , and V_{Mg}^{2+} is 0, 1 (spin-triplet), $1/2$ (spin-doublet), and 0 (spin-singlet), leading to the magnetic moments of 0, 2, 1, and 0 μ_B [70,71]. Thus, RTFM is associated with spin-triplet state when Mg-vacancy is introduced to MgO. Similar, effect of observation of RTFM is also predicted in CaO where the spin triplet state of Ca^{2+} is responsible for this effect [72,73]. Thus, Mg vacancies are required to sustain magnetism in this material. Hence, further attention was given to know the nature and stability of these vacancies in MgO in context of percolating magnetic order [70–77]. In this context, it was reported that the ground state configuration of bulk MgO with two Mg vacancies exhibits the energy difference of ~ 28 meV between ferromagnetic and antiferromagnetic states [74]. This energy difference is parallel to the thermal energy. Hence, magnetism cannot be sustained in MgO bulk at room temperature, even having Mg vacancies.

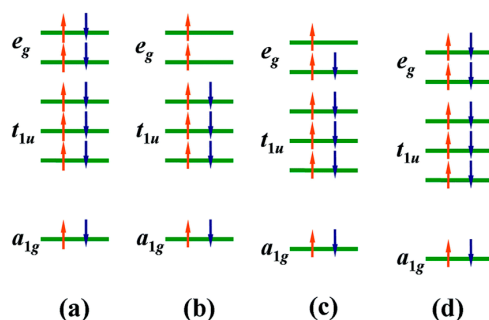


Figure 5. Schematic of single particle energy level diagram for (a) perfect MgO; (b) V_{Mg}^0 ; (c) V_{Mg} ; and (d) V_{Mg}^2 [71].

For legislating the persistence of magnetism, Wang et al., calculated Mg vacancy formation energy in MgO using density functional theory [74]. The values of Mg vacancy formation energy were 2.73 eV and 1.37 eV for MgO bulk and MgO quantum dots [74]. Thus, Mg vacancies occur in quantum dots due to low formation energy and lead to magnetism, as observed by various experimental reports [51–58]. In the case of MgO thin films, Mg vacancy formation energies are 2.45 and 2.74 eV for the surface and the subsurface layers, which are less than that of MgO bulk. Hence, thin films are another choice for occurrence of local magnetic moments, however, introduction of Mg vacancies is rather difficult. It is shown on the basis of molecular orbital diagrams of Mg-deficient clusters (Figure 6) that the occurrence of Mg-vacancies at the surface or near-surface of MgO clusters, a magnetic state ($S \geq 1$) becomes lower in total energy than the nonmagnetic singlet state ($S = 0$) by several eV. This leads to a spin-polarized ground state in MgO. The total spin of the clusters in their ground state is equal to the number of the surface Mg vacancies [76]. Thus, surface Mg vacancies play an important role for determining the magnetic properties of thin films.

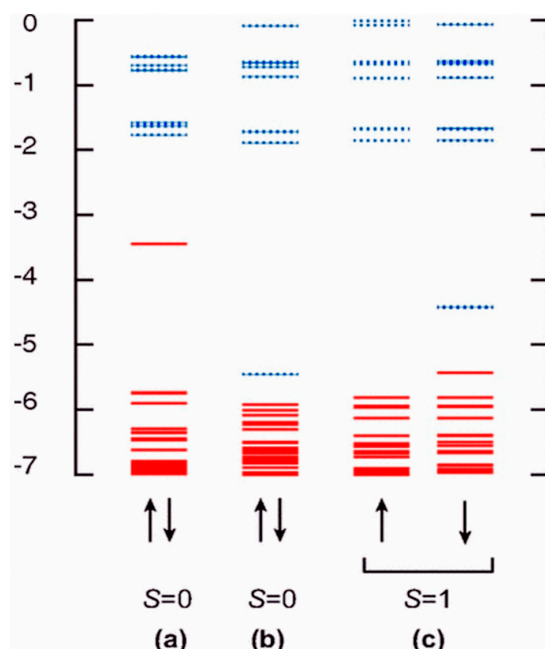


Figure 6. Molecular orbital energy-level diagram of occupied orbitals (solid lines) and unoccupied molecular orbitals (dotted lines) calculated for the $(4 \times 4 \times 4)$ -based clusters with one O or one Mg vacancy at the corner: (a) O-deficient $Mg_{32}O_{33}$ cluster in the spin-singlet state; (b) Mg-deficient $Mg_{31}O_{32}$ cluster in the spin-singlet state; and (c) Mg-deficient $Mg_{33}O_{32}$ cluster in the spin-triplet state [76].

Neutral (V_{Mg}^0) and singly-charged Mg vacancy (V_{Mg}^-) are responsible for the magnetic moment of MgO, which originates from the partially-occupied e_g orbitals, as discussed earlier. However, other defects, like closed shell Mg vacancy (V_{Mg}^{2-}), and V_{O}^0 , V_{O}^+ , and V_{O}^{2+} cannot lead to magnetic moments in MgO [70,71].

Apart from the origin of local magnetic moments in MgO by Mg vacancies, it will be important to know the mechanism of magnetic interactions. To understand this, let us consider the case of Mg vacancy. In the case of MgO, the neutral Mg vacancy has two holes trapped on oxygen neighbors [76]. This causes magnetic coupling to be induced through the p–p hybridization interaction of O atoms [73,74]. Thus, the magnetic moment in this material is induced by 2p orbitals of the nearest atoms surrounded by Mg vacancies, particularly $2p_{xy}$ makes a significant contribution [69]. Hence, magnetic interaction occurs through bond spin polarization between two Mg vacancies in MgO [74,76]. This kind of magnetic interaction is also reported for organic systems [77] and GaN [78].

4.2. Oxygen Vacancy/Composite Defects as a Source of Magnetism

Though O vacancy destroys the ferromagnetic ground state, experimental studies envisage an important role of oxygen vacancies to control magnetism in this material, as elaborated in previous section [51–53]. Thus, the theoretical investigations were carried out in this direction to revive the role of oxygen vacancies [79–83].

In general, oxygen vacancy formation energy in MgO is higher than that of Mg vacancy formation energy [74]. This envisages that the existence of oxygen vacancies is not preferred. In the case of the existence of oxygen vacancies, the magnetization is found to be independent of these vacancies. Theoretical investigations carried out by Sharma and Lowther suggest that the total magnetic moment of MgO substituted by N is found to be $1\mu_B$ [80]. Though oxygen vacancies exist in this N-substituted MgO system, no correlation between oxygen vacancies and saturation magnetization is observed [80]. In this case, composite defects, composed of an oxygen vacancy and a nitrogen-substituting oxygen, are responsible for magnetic behavior. Similar behavior is also reported when MgO is doped with boron and carbon [79]. Kuang et al. also reported that these composite defects promote magnetism in the case of oxygen vacancies [84]. It is contemplated that local magnetic moment is induced by the composite defects around the oxygen vacancy, when the exchange splitting of the oxygen vacancy is enhanced either by the hybridization between the N-p and nearest neighbor O-p orbitals or by applying on-site Coulomb repulsion and exchange interaction [81–83].

5. Magnetism of Radio-Frequency (RF) Sputtered MgO

In this context, we deposited MgO thin films by RF sputtering to explore the nature of defects. The detailed deposition procedure is published elsewhere [85]. The film is deposited on Si (100) substrate and annealed in situ at 700 °C for 3 h. In Figure 7a the high-resolution transmission electron microscopy (HRTEM) image of MgO thin film on Si substrate. HRTEM study was performed using Titan 80-300TM transmission electron microscope at Korea Institute of Science and Technology (KIST), Seoul, South Korea. The thickness of the deposited film is 18 nm. The magnetization (M) versus the applied magnetic field (H) curve of this film measured at room temperature is shown in Figure 7b. The behavior of the M-H curve is very similar to that already reported for MgO thin films of similar thickness [40,50–61]. This behavior reveals the onset of d^0 ferromagnetism in this film.

To obtain deeper insights on the source of magnetic behavior, near-edge X-ray absorption fine structure (NEXAFS) measurements were also performed at the 10 D KIST beamline (Pohang Accelerator Laboratory, Pohang, South Korea) in surface-sensitive, total electron yield (TEY) and bulk-sensitive, total fluorescence yield (TFY) modes at Mg K-edge and O K-edges for MgO thin films [86]. The instrumental details of beamline can be found elsewhere [87].

As mention earlier, the Mg ion is located at the center of a regular oxygen octahedron in MgO. Thus, the lowest empty Mg 3p orbitals should be degenerate to cause the sharp transition of electron from the Mg 1s orbital. As a result, spectral features of A_1 , A_2 , A_3 , A_4 , and A_5 appear in the Mg K-edge

spectra of MgO (Figure 8a) [88,89]. A visual inspection shows the presence of the same spectral features in the Mg K-edge spectra of both TEY and TFY modes for this film. This shows Mg co-ordination to be almost the same, both at the surface and in the volume of the film.

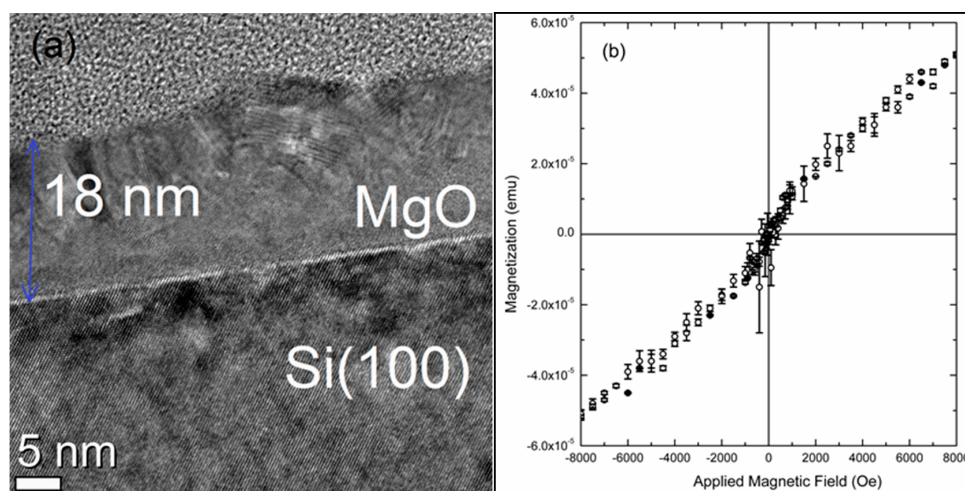


Figure 7. (a) High-resolution transmission electron micrograph, and (b) the M-H curve of the MgO thin film deposited using RF sputtering.

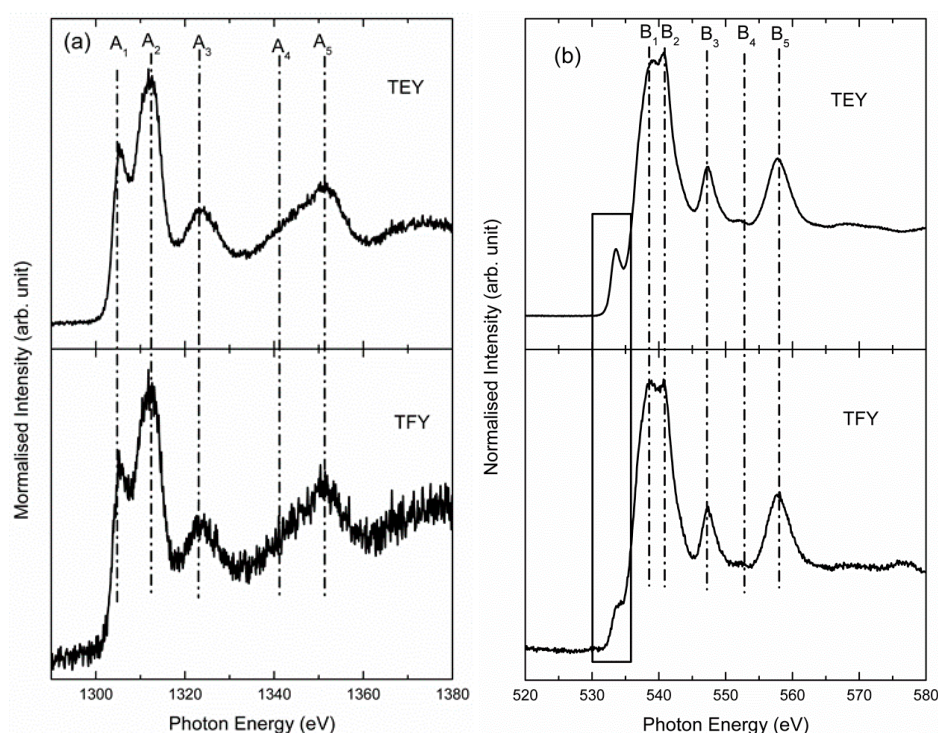


Figure 8. (a) Mg K-edge and (b) O K-edge spectra of the MgO thin film deposited using RF sputtering in TEY and TFY modes, respectively.

The measured O K-edge NEXAFS spectra [40,90–94] of the film detected by TEY and TFY [95] modes are shown in Figure 8b. According to electronic structure calculation the spectral features B₁, B₂, B₃, B₄ and B₅ in the energy range of 80 eV above threshold arise from multiple scattering resonances in the energy of the excited photoelectron in Mg and O states with p symmetry [40,90,92]. Rectangular region in Figure 8b shows pre-edge structures, which arises due to the excitation to the

localized bound state and presence of surface state or intermixing [92,96] as it is common to occur in the NEXAFS spectra of metal oxides. Concurrent with the Mg K-edge, the O K-edge spectral features are almost same for TEY and TFY modes. However, pre-edge region of the O K-edge spectrum exhibit a visual different both in shape and intensity. This indicates that oxygen has different electronic structure at surface and volume as the pre-edge reflects the presence of surface states. Since, the film is annealed at 700 °C for 3 h under vacuum of 10^{-7} Torr, the presence of oxygen vacancies are expected at the surface of the film and only oxygen vacancies are expected to cause magnetism in the present case. As discussed earlier, Mg vacancies play more dominant roles to determine the magnetism in this system rather than oxygen vacancies. Thus, composite defects play a role in this case.

6. Conclusions and Future Prospects

d^0 ferromagnetism occurs chiefly in non-magnetic oxide materials. These materials either contain completely filled d-/f-orbitals or unfilled d-/f-orbitals. Considering MgO as a prototype material for this category, it may be stated that this effect is induced by Mg vacancies above the threshold concentration of these defects. Contribution of these defects to this kind of magnetism is different when appearing at the surface and subsurface layers of the film. This behavior is associated with the spin triplet state of the Mg vacancy. Magnetic interaction occurs through-bond spin polarization between two Mg vacancies in MgO. Though oxygen vacancy does not induce magnetization, however, these vacancies can play important roles in doped systems and play significant roles in the case of doped MgO. As mention earlier, magnetism in these structures is induced by 2p orbitals of oxygen atoms surrounded by Mg vacancies and spin-triplet states. Measurements, like near edge fine structure, can open new pathways of understanding this kind of magnetism and give exact proof of the source of magnetism.

Acknowledgments: This work was supported by Korea Institute of Science and Technology, Seoul Korea (KIST project no.: 2V05210).

Author Contributions: Jitendra Pal Singh analyzed the data and wrote the paper, and Keun Hwa Chae helped collect related data and performed the final check on the manuscript. Both authors have read and approved the final manuscript.

Conflicts of Interest: Both authors declare no conflict of interest.

References

1. Cullity, B.D. *Introduction to Magnetic Materials*; Addison-Wesley: Massachusetts, MA, USA, 1972.
2. Qin, J.P.J.; Nogués, J.; Mikhaylova, M.; Roig, A.; Muñoz, J.S.; Muhammed, M. Differences in the magnetic properties of Co, Fe, and Ni 250–300 nm wide nanowires electrodeposited in amorphous anodized alumina templates. *Chem. Mater.* **2005**, *17*, 1829–1834. [[CrossRef](#)]
3. Singh, J.P.; Srivastava, R.C.; Agrawal, H.M.; Reddy, V.R.; Gupta, A. Observation of bulk like magnetic ordering below the blocking temperature in nanosized zinc ferrite. *J. Magn. Magn. Mater.* **2012**, *324*, 2553–2559. [[CrossRef](#)]
4. Chetri, P.; Choudhury, B.; Choudhury, A. Room temperature ferromagnetism in SnO₂ nanoparticles: An experimental and density functional study. *J. Mater. Chem. C* **2014**, *2*, 9294–9302. [[CrossRef](#)]
5. Díaz-Gallifa, P.; Fabelo, O.; Pasán, J.; Cañadillas-Delgado, L.; Lloret, F.; Julve, M.; Ruiz-Pérez, C. Two-Dimensional 3d–4f Heterometallic Coordination Polymers: Syntheses, Crystal Structures, and Magnetic Properties of Six New Co(II)–Ln(III) Compounds. *Inorg. Chem.* **2014**, *53*, 6299–6308. [[CrossRef](#)] [[PubMed](#)]
6. Venkatesan, M.; Fitzgerald, C.B.; Coey, J.M.D. Thin films: Unexpected magnetism in a dielectric oxide. *Nature* **2004**, *430*, 630. [[CrossRef](#)] [[PubMed](#)]
7. Si, M.S.; Gao, D.; Yang, D.; Peng, Y.; Zhang, Z.Y.; Xue, D.; Liu, Y.; Deng, X.; Zhang, G.P. Intrinsic ferromagnetism in hexagonal boron nitride nanosheets. *J. Chem. Phys.* **2014**, *140*, 204701. [[CrossRef](#)] [[PubMed](#)]
8. Wang, Y.; Li, L.; Prucnal, S.; Chen, X.; Tong, W.; Yang, Z.; Munnik, F.; Potzger, K.; Skorupa, W.; Gemming, S.; et al. Disentangling defect-induced ferromagnetism in SiC. *Phys. Rev.* **2014**, *89*, 014417. [[CrossRef](#)]

9. Sundaresan, A.; Rao, C.N.R. Ferromagnetism as a universal feature of inorganic nanoparticles. *Nano Today* **2009**, *4*, 96–106. [[CrossRef](#)]
10. Rao, C.N.; Nakate, U.T.; Choudhary, R.J.; Kale, S.N. Defect-induced magneto-optic properties of MgO nanoparticles realized as optical-fiber-based low-field magnetic sensor. *Appl. Phys. Lett.* **2013**, *103*, 151107. [[CrossRef](#)]
11. Zhang, J.; Gao, D.; Si, M.; Zhu, Z.; Yang, G.; Shia, Z.; Xue, D. Origin of the unexpected room temperature ferromagnetism: formation of artificial defects on the surface in NaCl particles. *J. Mater. Chem. C* **2013**, *1*, 6216–6222. [[CrossRef](#)]
12. Ma, Y.W.; Lu, Y.H.; Yi, J.B.; Feng, Y.P.; Herng, T.S.; Liu, X.; Gao, D.Q.; Xue, D.S.; Xue, J.M.; Ouyang, J.Y.; et al. Room temperature ferromagnetism in teflon due to carbon dangling bonds. *Nat. Commun.* **2012**, *3*, 1–8. [[CrossRef](#)] [[PubMed](#)]
13. Xu, K.; Li, X.; Chen, P.; Zhou, D.; Wu, C.; Guo, Y.; Zhang, L.; Zhao, J.; Wu, X.; Xi, Y. Hydrogen dangling bonds induce ferromagnetism in two-dimensional metal-free graphitic-C₃N₄ nanosheets. *Chem. Sci.* **2015**, *6*, 283–287. [[CrossRef](#)] [[PubMed](#)]
14. Giesbers, A.J.M.; Uhlířová, K.; Konečný, M.; Peters, E.C.; Burghard, M.; Aarts, J.; Flipse, C.F.J. Interface-induced room-temperature ferromagnetism in hydrogenated epitaxial grapheme. *Phys. Rev. Lett.* **2013**, *111*, 166101. [[CrossRef](#)] [[PubMed](#)]
15. Dimri, M.C.; Khanduri, H.; Kooskora, H.; Kodu, M.; Jaaniso, R.; Heinmaa, I.; Mere, A.; Krustok, J.; Stern, R. Room-temperature ferromagnetism in Ca and Mg stabilized cubic zirconia bulk samples and thin films prepared by pulsed laser deposition. *J. Phys. D Appl. Phys.* **2012**, *45*, 475003. [[CrossRef](#)]
16. Glinchuk, M.D.; Eliseev, E.A.; Khist, V.V.; Morozovska, A.N. Ferromagnetism induced by magnetic vacancies as a size effect in thin films of nonmagnetic oxides. *Thin Solid Films* **2013**, *534*, 685–692. [[CrossRef](#)]
17. Gao, D.; Zhang, J.; Jing, J.Z.; Zhaohui, Q.; Shi, W.; Shi, H.; Xue, D. Vacancy-Mediated Magnetism in Pure Copper Oxide Nanoparticles. *Nanoscale Res. Lett.* **2010**, *5*, 769–772. [[CrossRef](#)] [[PubMed](#)]
18. Thurber, A.P.; Alanko, G.; Beausoleil, G.L., II; Dodge, K.N.; Hanna, C.B.; Punnoose, A. Unusual crystallite growth and modification of ferromagnetism due to aging in pure and doped ZnO nanoparticles. *J. Appl. Phys.* **2012**, *111*, 07C319. [[CrossRef](#)]
19. Peng, H.; Xiang, H.J.; Wei, S.H.; Li, S.S.; Xia, J.B.; Li, J. Origin and enhancement of hole-induced ferromagnetism in first-row d⁰ semiconductors. *Phys. Rev. Lett.* **2009**, *102*, 017201. [[CrossRef](#)] [[PubMed](#)]
20. Gao, D.; Zhang, J.; Yang, G.; Qi, J.; Si, M.; Xue, D. Ferromagnetism Induced by Oxygen Vacancies in Zinc Peroxide Nanoparticles. *J. Phys. Chem. C* **2011**, *115*, 16405–16410. [[CrossRef](#)]
21. Chen, S.Y.; Lu, Y.H.; Huang, T.W.; Yan, D.C.; Dong, C.L. Oxygen Vacancy Dependent Magnetism of CeO₂ Nanoparticles Prepared by Thermal Decomposition Method. *J. Phys. Chem. C* **2010**, *114*, 19576–19581. [[CrossRef](#)]
22. Yang, Z.; Gao, D.; Tao, K.; Zhang, J.; Shi, Z.; Xu, Q.; Shia, S.; Xue, D. A series of unexpected ferromagnetic behaviors based on the surface-vacancy state: An insight into NiO nanoparticles with a core-shell structure. *RSC Adv.* **2014**, *4*, 46133–46140. [[CrossRef](#)]
23. Zhou, B.; Wu, P.; Zhou, W. Tunable bandgap and ferromagnetism in sputtered epitaxial Sn_{1-x}Mg_xO₂ thin films. *Appl. Phys. Lett.* **2012**, *101*, 182406. [[CrossRef](#)]
24. Hua, P.; Sha, Z.; Fa-Shen, L. Electronic structures and magnetic couplings of B-, C-, and N-doped BeO. *Chin. Phys. B* **2013**, *22*, 047504. [[CrossRef](#)]
25. Farvid, S.S.; Sabergharesou, T.; Hutfluss, L.N.; Hegde, M.; Prouzet, E.; Radovanovic, P.V. Evidence of charge-transfer ferromagnetism in transparent diluted magnetic oxide nanocrystals: Switching the mechanism of magnetic interactions. *J. Am. Chem. Soc.* **2014**, *136*, 7669–7679. [[CrossRef](#)] [[PubMed](#)]
26. Pemmaraju, C.D.; Sanvito, S. Ferromagnetism driven by intrinsic point defects in HfO₂. *Phys. Rev. Lett.* **2005**, *94*, 217205. [[CrossRef](#)] [[PubMed](#)]
27. Mellor, J.W. *A Comprehensive Treatise on Inorganic and Theoretical Chemistry*; Longmans: London, UK, 1924; pp. 280–284.
28. Verma, N.K.; Verma, N. *Academic Chemistry IX*; Laxmi Publications: New Delhi, India, 2012.
29. Chang, K.J.; Cohen, M.I. High-pressure behavior of MgO: Structural and electronic properties. *Phys. Rev. B* **2008**, *30*, 4774–4781. [[CrossRef](#)]

30. Magnesium oxide (MgO) crystal structure, lattice parameters, thermal expansion. In *II-VI and I-VII Compounds; Semimagnetic Compounds*; Madelung, O., Rössler, U., Schulz, M., Eds.; Springer: Berlin/Heidelberg, Germany, 1999; Volume 41B, pp. 1–6.
31. Lempicki, A. The Electrical Conductivity of MgO Single Crystals at High Temperatures. *Proc. Phys. Soc. B* **1953**, *66*, 281–283. [[CrossRef](#)]
32. Wilson, I.O. Magnesium oxide as a high-temperature insulant. *IEE Proc.* **1981**, *128*, 159–164. [[CrossRef](#)]
33. Yamaka, K.; Sawamoto, K. Photoinduced Hall effect in MgO. *Phys. Rev.* **1956**, *101*, 565–566. [[CrossRef](#)]
34. Reiling, G.H.; Henslzy, E. Fundamental optical absorption in magnesium oxide. *Phys. Rev.* **1958**, *112*, 1106–1111. [[CrossRef](#)]
35. Subramanian, M.A.; Shannon, R.D.; Chai, B.H.T.; Abraham, M.M.; Wintersgil, M.C. Dielectric Constants of BeO, MgO, and CaO Using the Two-Terminal Method. *Phys. Chem. Miner.* **1989**, *16*, 741–746. [[CrossRef](#)]
36. Singh, J.P.; Kaur, B.; Gautam, S.; Lim, W.C.; Asokan, K.; Chae, K.H. Chemical effects at interfaces of Fe/MgO/Fe magnetic tunnel junction. *Superlattices Microstruct.* **2016**, *100*, 560–586. [[CrossRef](#)]
37. Liu, J.; Wang, W.; Guo, Z.; Zeng, R.; Dou, S.; Chen, X. Peashell-like nanostructure—A new kind of one-dimensional nanostructure: The case of magnesium oxide. *Chem. Commun.* **2010**, *46*, 3887–3889. [[CrossRef](#)] [[PubMed](#)]
38. Singh, J.P.; Won, S.O.; Lim, W.C.; Shim, C.H.; Chae, K.H. Optical behavior of MgO nanoparticles investigated using diffuse reflectance and near edge X-ray absorption spectroscopy. *Mater. Lett.* **2017**, *198*, 34–37. [[CrossRef](#)]
39. Uchino, T.; Okutsu, D. Broadband laser emission from color centers inside MgO microcrystals. *Phys. Rev. Lett.* **2008**, *101*, 117401. [[CrossRef](#)] [[PubMed](#)]
40. Singh, J.P.; Chen, C.L.; Dong, C.L.; Prakash, J.; Kabiraj, D.; Kanjilal, D.; Pong, W.F.; Asokan, K. Role of surface and subsurface defects in MgO thin film: XANES and magnetic investigations. *Superlattice Microstruct.* **2015**, *77*, 313–324. [[CrossRef](#)]
41. Wu, Y.Z.; Schmid, A.K.; Qiu, Z.Q. Spin-Dependent Quantum Interference from Epitaxial MgO Thin Films on Fe(001). *Phys. Rev. Lett.* **2006**, *97*, 217205. [[CrossRef](#)] [[PubMed](#)]
42. Jambois, O.; Carreras, P.; Antony, A.; Bertomeu, J.; Martínez-Boubeta, C. Resistance switching in transparent magnetic MgO films. *Solid State Commun.* **2011**, *151*, 1856–1859. [[CrossRef](#)]
43. Nomura, K.; Taya, S.; Okazawa, A.; Kojima, N. Sol-gel synthesis and dilute magnetism of nano MgO powder doped with Fe. *Hyperfine Interact.* **2014**, *226*, 161–169. [[CrossRef](#)]
44. Ramachandran, S.; Narayan, J.; Prater, J.T. Magnetic properties of Ni-doped MgO diluted magnetic insulators. *Appl. Phys. Lett.* **2007**, *90*, 132511. [[CrossRef](#)]
45. Narayan, J.; Nori, S.; Pandya, D.K.; Avasthi, D.K.; Smirnov, A.I. Defect dependent ferromagnetism in MgO doped with Ni and Co. *Appl. Phys. Lett.* **2008**, *93*, 082507. [[CrossRef](#)]
46. Chun-Ming, L.; Hai-Quan, G.; Xia, X.; Yan, Z.; Yong, J.; Meng, C.; Xiao-Tao, Z. Optical and magnetic properties of nitrogen ion implanted MgO single crystal. *Chin. Phys. B* **2011**, *20*, 047505. [[CrossRef](#)]
47. Li, Y.; Deng, R.; Yao, B.; Xing, G.; Wang, D.; Wu, T. Tuning ferromagnetism in Mg_xZn_{1-x}O thin films by band gap and defect engineering. *Appl. Phys. Lett.* **2010**, *97*, 102506. [[CrossRef](#)]
48. Mishra, D.; Mandal, B.P.; Mukherjee, R.; Naik, R.; Lawes, G.; Nadgorny, B. Oxygen vacancy enhanced room temperature magnetism in Al-doped MgO nanoparticles. *Appl. Phys. Lett.* **2013**, *102*, 182404. [[CrossRef](#)]
49. Li, Q.; Ye, B.; Hao, Y.; Liu, J.; Zhang, J.; Zhang, L.; Kong, W.; Weng, H.; Ye, B. Room-temperature ferromagnetism observed in C-/N-/O-implanted MgO single crystals. *Chem. Phys. Lett.* **2013**, *556*, 237–241. [[CrossRef](#)]
50. Kumar, P.; Singh, B.; Singh, J.P.; Kumar, A.; Chae, K.H.; Asokan, K.; Kanjilal, D. Room temperature ferromagnetism in MgO single crystals via N-implantation. In Proceedings of the International Conference on Nano Structuring by Ion Beam, Indore, India, 11–13 October 2017; p. 40.
51. Araujo, C.M.; Kapilashrami, M.; Jun, X.; Jayakumar, O.D.; Nagar, S.; Wu, Y.; Århammar, C.; Johansson, B.; Belova, L.; Ahuja, R.; et al. Room temperature ferromagnetism in pristine MgO thin films. *Appl. Phys. Lett.* **2010**, *96*, 232505. [[CrossRef](#)]
52. Kapilashrami, M.; Xu, J.; Rao, K.V.; Belova, L.; Carlegrim, E.; Fahlman, M. Experimental evidence for ferromagnetism at room temperature in MgO thin films. *J. Phys. Condens. Matter* **2010**, *22*, 345004. [[CrossRef](#)] [[PubMed](#)]
53. Wu, Y.; Zhan, Y.; Fahlman, M.; Fang, M.; Rao, K.V.; Belova, L. In-situ solution processed room temperature ferromagnetic MgO thin films printed by inkjet technique. *MRS Proc.* **2011**, *1292*, 12–26. [[CrossRef](#)]

54. Li, J.; Jiang, Y.; Li, Y.; Yang, D.; Xu, Y.; Yan, M. Origin of room temperature ferromagnetism in MgO films. *Appl. Phys. Lett.* **2013**, *102*, 072406. [[CrossRef](#)]
55. Choudhury, B.; Choudhury, A. Microstructural, optical and magnetic properties study of nanocrystalline MgO. *Mater. Res. Exp.* **2014**, *1*, 025026. [[CrossRef](#)]
56. Hu, J.; Zhang, Z.; Zhao, M.; Qin, H.; Jiang, M. Room-temperature ferromagnetism in MgO nanocrystalline powders. *Appl. Phys. Lett.* **2008**, *93*, 192503. [[CrossRef](#)]
57. Kumar, N.; Jagadeesan, D.; Pillai, P.B.; Chacko, M.; Eswaramoorthy, M.; Sundaresan, A. Ferromagnetism in thin-walled hollow spheres of non-magnetic inorganic materials. *Chem. Phys. Lett.* **2011**, *504*, 189–192. [[CrossRef](#)]
58. Mahadeva, S.K.; Fan, J.; Biswas, A.; Sreelath, K.S.; Belova, L.; Rao, K.V. Magnetism of amorphous and nano-crystallized DC-sputter deposited MgO thin films. *Nanomater* **2013**, *3*, 486–497. [[CrossRef](#)] [[PubMed](#)]
59. Kumar, A.; Kumar, J.; Priya, S. Defect and adsorbate induced ferromagnetic spin-order in magnesium oxide nanocrystallites. *Appl. Phys. Lett.* **2012**, *100*, 192404. [[CrossRef](#)]
60. Maoz, B.M.; Tirosh, E.; Sadan, M.B.; Markovich, G. Defect-induced magnetism in chemically synthesized nanoscale sheets of MgO. *Phys. Rev. B* **2011**, *83*, 161201(R). [[CrossRef](#)]
61. Balcells, L.; Beltrán, J.I.; Martínez-Boubeta, C.; Konstantinović, Z.; Arbiol, J.; Martínez, B. Aging of magnetic properties in MgO films. *Appl. Phys. Lett.* **2011**, *97*, 252503. [[CrossRef](#)]
62. Liu, G.; Ji, S.; Yin, L.; Fei, G.; Ye, C. An investigation of the electronic properties of MgO doped with group III, IV, and V elements: Trends with varying dopant atomic number. *J. Phys. Condens. Matter* **2010**, *22*, 046002. [[CrossRef](#)] [[PubMed](#)]
63. Chen, Y.; Yang, J.; Mi, W.; Song, Q.; Yan, H. Ferromagnetism in Cu-doped MgO: Density-functional calculations. *Solid State Commun.* **2014**, *194*, 1–5. [[CrossRef](#)]
64. Beltrána, J.I.; Montyb, C.; Balcellsc, L.; Martínez-Boubetad, C. Possible d⁰ ferromagnetism in MgO. *Solid State Commun.* **2009**, *149*, 1654–1657. [[CrossRef](#)]
65. Volnianska, O.; Boguslawski, P. Magnetism of solids resulting from spin polarization of p orbitals. *J. Phys. Condens. Matter* **2010**, *22*, 073202. [[CrossRef](#)] [[PubMed](#)]
66. Pardo, V.; Pickett, W.E. Magnetism from 2p states in alkaline earth monoxides: Trends with varying N impurity concentration. *Phys. Rev. B* **2008**, *78*, 134427. [[CrossRef](#)]
67. Seike, M.; Dinh, V.A.; Fukushima, T.; Sato, K.; Katayama-Yoshida, H. Self-organized nanostructures and high blocking temperatures in MgO-based d⁰ ferromagnets. *Jpn. J. Appl. Phys.* **2012**, *51*, 050201. [[CrossRef](#)]
68. Seike, M.; Sato, K.; Yoshida, H.K. The magnetic properties of hole-doped MgO. *Jpn. J. Appl. Phys.* **2011**, *50*, 090204. [[CrossRef](#)]
69. Kim, D.; Yang, J.; Hong, J. Mg Vacancy Defect Induced Half Metallic MgO(001) Film. *J. Korean Phys. Soc.* **2010**, *56*, L1729–L1732. [[CrossRef](#)]
70. Droghetti, A.; Pemmaraju, C.D.; Sanvito, S. Polaronic distortion and vacancy-induced magnetism in MgO. *Phys. Rev. B* **2010**, *81*, 092403. [[CrossRef](#)]
71. Kuang, F.-G.; Kang, S.-Y.; Kuang, X.-Y.; Cheng, Q.-F. An ab initio study on the electronic and magnetic properties of MgO with intrinsic defects. *RSC Adv.* **2014**, *4*, 51366. [[CrossRef](#)]
72. Osorio-Guill'en, J.; Lany, S.; Barabash, S.V.; Zunger, A. Magnetism without magnetic ions: percolation, exchange, and formation energies of magnetism-promoting intrinsic defects in CaO. *Phys. Rev. Lett.* **2006**, *96*, 107203. [[CrossRef](#)] [[PubMed](#)]
73. McKenna, K.P.; Shluger, A.L. First-principles calculations of defects near a grain boundary in MgO. *Phys. Rev. B* **2009**, *79*, 224116. [[CrossRef](#)]
74. Wang, F.; Pang, Z.; Lin, L.; Fang, S.; Dai, Y.; Han, S. Magnetism in undoped MgO studied by density functional theory. *Phys. Rev. B* **2009**, *80*, 144424. [[CrossRef](#)]
75. Stoneham, A.M.; Pathak, A.P.; Bartram, R.H. The ground state of two-hole centres in oxide. *J. Phys. C: Solid State Phys.* **1976**, *9*, 73–80. [[CrossRef](#)]
76. Uchino, T.; Yoko, T. Spin-polarized ground states and ferromagnetic order induced by low-coordinated surface atoms and defects in nanoscale magnesium oxide. *Phys. Rev. B* **2013**, *87*, 144414. [[CrossRef](#)]
77. Yoshizawa, K.; Kuga, T.; Sato, T.; Hatanaka, M.; Tanaka, K.; Yamabe, T. Through-Bond and Through-Space Interactions of Organic Radicals Coupled by m-Phenylene. *Bull. Chem. Soc. Jpn.* **1996**, *69*, 3443–3450. [[CrossRef](#)]

78. Jin, H.; Dai, Y.; Huang, B.B.; Whangbo, M.-H. Ferromagnetism of undoped GaN mediated by through-bond spin polarization between nitrogen dangling bonds. *Appl. Phys. Lett.* **2009**, *94*, 162505. [CrossRef]
79. Bannikov, V.; Shein, I.R.; Ivanovskii, A.L. Novel magnetic half-metallic materials based on ionic insulators doped with nonmagnetic impurities: MgO + B, C, N Systems. *Tech. Phys. Lett.* **2007**, *33*, 541–544. [CrossRef]
80. Sharma, V.; Lowther, J.E. Ferromagnetism in nitrogen doped oxide: A first principle study. *J. Nano-Electron. Phys.* **2011**, *3*, 453–459.
81. Zhang, Y.F.; Feng, M.; Shao, B.; Lu, Y.; Liu, H.; Zuo, X. Ab initio calculations on magnetism induced by composite defects in magnesium oxide. *J. Appl. Phys.* **2014**, *115*, 17A926. [CrossRef]
82. Mir, A.; Bekkouche, B.; Boukortt, A.; Kacimi, S.; Djermouni, M.; Zaoui, A. Enhancement of ferromagnetic ordering curie temperature in N-doped MgO under hydrostatic pressure. *Model. Numer. Simul. Mater. Sci.* **2012**, *2*, 37–42. [CrossRef]
83. Pesci, M.; Gallino, F.; Valentin, C.D.; Pacchioni, G. Nature of defect states in nitrogen-doped MgO. *J. Phys. Chem. C* **2010**, *114*, 1350–1356. [CrossRef]
84. Kuang, F.-G.; Kang, S.-Y.; Xu, Y.-Q.; Xiong, Z.-Z.; Liao, J.-F.; Yu, H.-J.; Zhang, X.-K.; Sun, T.-Z.; Cao, J. Effect of oxygen and magnesium vacancies on the d^0 magnetism of C-monodoped MgO using ab initio method. *J. Alloys Compd.* **2017**, *712*, 526–534. [CrossRef]
85. Singh, J.P.; Kumar, M.; Lee, I.J.; Chae, K.H. X-ray reflectivity and near edge X-ray absorption fine structure investigations of MgO thin films. *Appl. Sci. Lett.* **2017**, in press.
86. Singh, J.P.; Lin, W.C.; Lee, J.; Song, J.; Lee, I.J.; Chae, K.H. Surface and local electronic structure modification of MgO film using Zn and Fe ion implantation. *Appl. Surface Sci.* **2017**, in press. [CrossRef]
87. Hwang, H.-N.; Kim, H.-S.; Kim, B.; Hwang, C.C.; Moon, S.W.; Chung, S.M.; Jeon, C.; Park, C.-Y.; Chae, K.H.; Choi, W.K. Construction of a soft X-ray beamline at the PLS. *Nucl. Instrum. Method. Phys. Res. A* **2007**, *581*, 850–855. [CrossRef]
88. Yoshida, T.; Tanaka, T.; Yoshida, H.; Funabiki, T.; Yoshida, S. Study of Dehydration of Magnesium Hydroxide. *J. Phys. Chem.* **1995**, *99*, 10890–10896. [CrossRef]
89. Singh, J.P.; Gautam, S.; Singh, B.B.; Chaudhary, S.; Kabiraj, D.; Kanjilal, D.; Chae, K.H.; Kotnala, R.; Lee, J.-M.; Chen, J.-M.; et al. Magnetic, electronic structure and interface study of Fe/MgO/Fe multilayer. *Adv. Mater. Lett.* **2014**, *5*, 372–377. [CrossRef]
90. McLeod, J.A.; Wilks, R.G.; Skorikov, N.A.; Finkelstein, L.D. Bandgaps and Electronic Structure of Alkaline Earth and Post-Transition Metal Oxides. *Phys. Rev. B* **2010**, *81*, 245123. [CrossRef]
91. Singh, J.P.; Sulania, I.; Prakash, J.; Gautam, S.; Chae, K.H.; Kanjilal, D.; Asokan, K. Study of surface morphology and grain size of irradiated MgO thin films. *Adv. Mater. Lett.* **2012**, *3*, 112–117. [CrossRef]
92. Linder, T.; Sauer, H.; Engel, W.; Kmabe, K. Near-edge structure in electron-energy-loss spectra of MgO. *Phys. Rev. B* **2006**, *33*, 22–24. [CrossRef]
93. Bianconi, A. Surface X-Ray absorption spectroscopy: Surface EXAFS and surface XANES. *Appl. Surf. Sci.* **1980**, *63*, 392–418. [CrossRef]
94. Garcia, J.; Bianconi, A.; Benfatto, M.; Natoli, C.R. Coordination geometry of transition metal ions in dilute solutions by XANES. *J. Phys. Colloq.* **1986**, *47*, C8-49-C8-54. [CrossRef]
95. Bianconi, A.; Marcelli, A. *Synchrotron Radiation Research: Advances in Surface and Interface Science Techniques*; Springer: Boston, MA, USA, 1992.
96. Bianconi, A. Core excitons and inner well resonances in surface soft x-ray absorption (SSXA) spectra. *Surf. Sci.* **1979**, *89*, 41–50. [CrossRef]

